Minireview

Interpretation of anatomic correlates of outer retinal bands in optical coherence tomography

Xincheng Yao[1,2] (ID)**, Taeyoon Son[1]** (ID)**, Tae-Hoon Kim[1]** (ID) **and David Le[1]** (ID)

[1]Department of Bioengineering, University of Illinois at Chicago, Chicago, IL 60607, USA; [2]Department of Ophthalmology and Visual Sciences, University of Illinois at Chicago, Chicago, IL 60612, USA
Corresponding author: Xincheng Yao. Email: xcy@uic.edu

Impact statement

A better understanding of anatomic correlates of image features is essential for accurate interpretation of clinical outcomes. This article summarizes interpretations of anatomic correlates of outer retinal bands in optical coherence tomography (OCT). Quantitative analysis is conducted to establish the correlation between the OCT bands and retinal histology.

Abstract

By providing the sectioning capability to differentiate individual retinal layers, optical coherence tomography (OCT) is revolutionizing eye disease diagnosis and treatment evaluation. A better understanding of the hyper- and hypo-reflective bands in retinal OCT is essential for accurate interpretation of clinical outcomes. In this article, we summarize the interpretations of clinical OCT and adaptive optics (AO) OCT (AO-OCT) of the outer retina in the human eye, and briefly review OCT investigation of the outer retina in animal models. Quantitative analysis of outer retinal OCT bands is compared to established parameters of retinal histology. The literature review and comparative analysis support that both inner/outer segment (IS/OS) junction and IS ellipsoid zone nonexclusively contribute to the second band; and OS, OS tips, and retinal pigment epithelium apical processes contribute to the third band in conventional OCT. In contrast, AO-OCT might predominantly detect the IS/OS junction and OS tip signals at the second and third bands due to its improved sectioning capability and possible AO effect on the sensitivities for recording ballistic and diffusive photons from different regions of the outer retina.

Keywords: Retina, photoreceptor, optical coherence tomography (OCT), outer segment (OS), inner segment (IS), ellipsoid, mitochondria

Introduction

By providing the unparalleled capability for imaging individual retinal layers, optical coherence tomography (OCT) is revolutionizing eye disease diagnosis and treatment evaluation. An in-depth understanding of the hyper- and hypo-reflective bands in retinal OCT is essential for accurate interpretation of clinical outcomes. Four hyper-reflective OCT bands are typically observed at the outer retina of the human eye (Figure 1(a)). The interpretations of the first and fourth bands are relatively consistent, but the second and third bands remain a great controversy.[1–3]

The first band is commonly attributed to the external limiting membrane (ELM).[1–4] The ELM, also named as the outer limiting membrane (OLM), is the line formed by junctional complexes between Müller cells and photoreceptor inner segments (IS)[5] (Figure 1(b)). The ELM is not only playing a role in maintaining the structure of the retina through mechanical strength but also one part of the retinal barrier, which can be disrupted in pathological conditions.[6] Changes in the ELM have been observed in age-related macular degeneration,[7] diabetic macular edema,[8,9] Stargardt disease,[10] myopic choroidal neovascularization,[11] and macular hole.[12]

The fourth band has been named retinal pigment epithelium (RPE)/Bruch's complex.[13] There is no doubt that the RPE is the major contributor with potential contributions from Bruch's membrane and choriocapillaris.[14] The fourth band can be occasionally seen as two distinctive hyper-reflective bands, particularly when pathology is
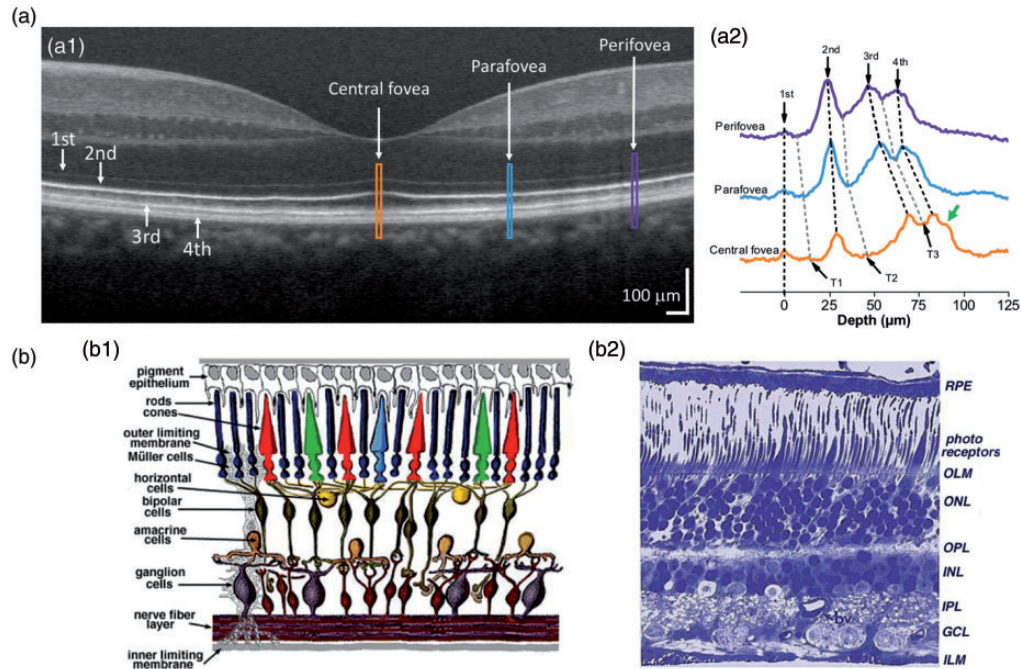
Figure 1. (a) Representative OCT B-scan of the human retina (a1) and reflectance profiles (a2) of the central fovea (yellow), parafovea (blue), and perifovea (purple). Yellow, blue, and purple windows in (a1) indicate retinal regions for comparative reflectance profile analysis. The first band locations of the three profiles are aligned together to show the relative distances of the second, third, and fourth bands. The green arrow near the fourth band in the central fovea indicates a possible fifth band, i.e. Bruch's membrane. T1–T3 indicate trough positions along the reflectance profiles. (b) Representative schematic diagram (b1) and histological micrograph (b2) of the retina. (A color version of this figure is available in the online journal.)
Source: Figure a1 and a2 are from Xincheng Yao's lab image gallery. Figure b1 and b2 are reprinted with permission from Simple Anatomy of the Retina.[5]
RPE: retinal pigment epithelium; OLM: outer limiting membrane; ONL: outer nuclear layer; OPL: outer plexiform layer; INL: inner nuclear layer; IPL: inner plexiform layer; GCL: ganglion cell layer; ILM: inner limiting membrane.

present.[15–19] Bruch's membrane is a 2–4 μm thick acellular matrix between the RPE and choroid.[20] Since clinical OCT instruments typically provide axial resolutions 5–10 μm, accurate segmentation of Bruch's membrane under normal conditions is still challenging.

Comparative alignment of the outer retinal OCT bands with an anatomically correct model suggested the IS ellipsoid (ISe) and interdigitation zone (IZ) as the correlates to the second and third bands,[1] and the *2014 International OCT Nomenclature Meeting* affirmed the ISe and IZ as the anatomic correlates of the second and third bands.[13] OCT study of animal retinas further provided experimental evidence to support the ISe as a contributor to the second band.[21,22] Based on the international OCT nomenclature for the human retina,[13] a uniform standard for rodent OCT layer nomenclature has been recently reported.[23] However, adaptive optics (AO) OCT (AO-OCT) study revealed that the second band thickness is much thinner than the ISe thickness.[2] In addition to the IZ interpretation for the third band, outer segment (OS) tips[2] and the RPE phagosomes[3] have also been proposed as alternative candidates. Therefore, anatomic sources of the second and third bands are still controversial, and the different observations between the clinical OCT and AO-OCT are not well understood. In this article, we summarize the band interpretations of clinical OCT and AO-OCT and conduct quantitative analysis to establish the correlation of each band to the outer retina.

Clinical OCT of the outer retina

Both the IS/OS junction and ISe have been proposed as anatomic sources of the second band. Based on a comprehensive literature review and analysis of retinal histology, an anatomically correct scale model has been developed for comparative analysis of the OCT bands of the outer retina.[1] Figure 2(a) and (b) illustrates scale drawings of the outer retina at central foveal and perifoveal regions, respectively. Figure 3(a) and (b) shows the comparative alignment of clinical OCT bands with the anatomic model at central foveal (Figure 3(a)) and perifoveal (Figure 3(b)) regions. As shown in Figure 3, the second band matches the ISe region; the third band matches the contact cylinder, later renamed as the IZ;[13] and the fourth band matches the RPE, later renamed as RPE/Bruch's complex.[13]

The IS consists of two parts, the myoid (ELM side) and the ellipsoid (OS side). As shown in Table 1, the average lengths of the IS myoid (ISm), ISe, and OS are reported as 14, 20, and 35 μm, respectively, at the central fovea.[1,24] In other words, the IS (34 μm) and OS (35 μm) lengths are almost equal at the central fovea. Therefore, if the second band is only attributed to the IS/OS junction, it is expected to see the second band at the midway point between the first and third bands in Figure 3(a). However, the second band is unambiguously closer to the first band, i.e. the ELM, compared to the distance to the "3 + 4" band in Figure 3(a). Likewise, in Figure 1(a), the second band is
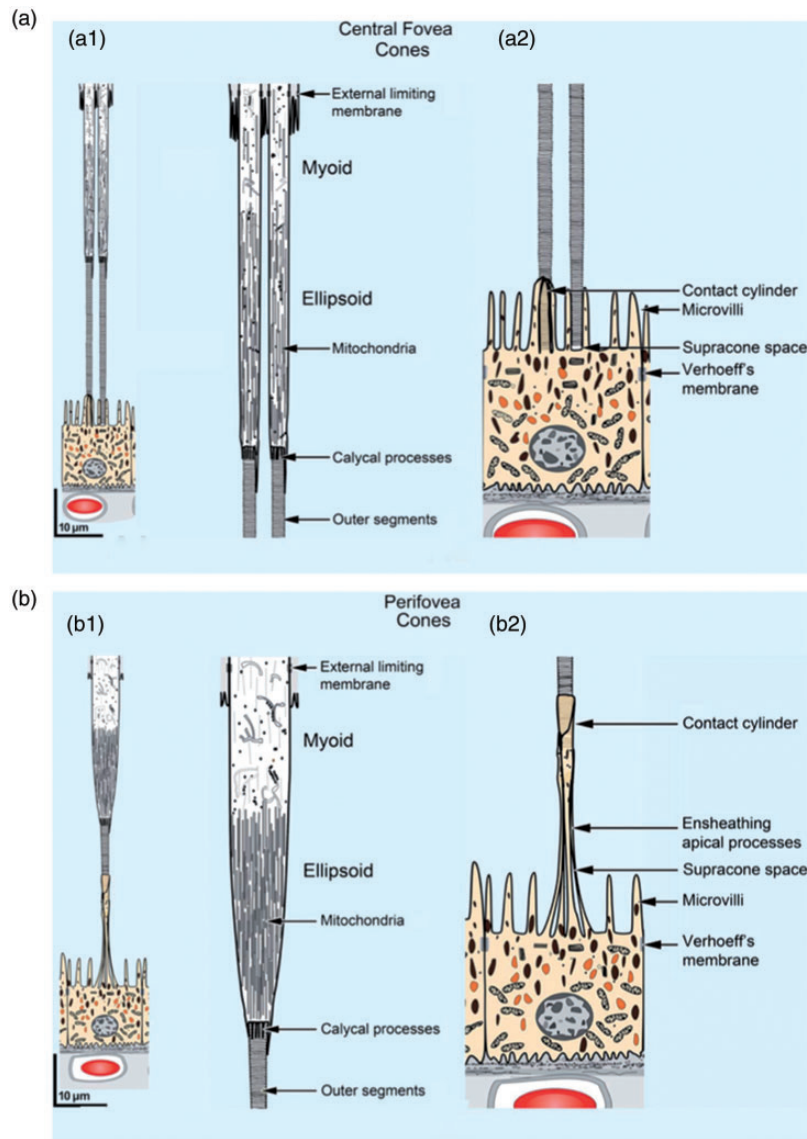
Figure 2. Scale drawings of the outer retina at central foveal (a) and perifoveal (b) regions. (a1/b1) show low magnification illustration, and (a2/b2) show high magnification illustration in two parts of the anatomically correct model. (A color version of this figure is available in the online journal.)
Source: Modified with permission from Spaide and Curcio.[1]

located closer to the first band than the third band at the central fovea. The third and fourth bands in Figure 3(a) are blended due to the limited axial resolution. Recent OCT resolution improvement enables differentiation of the third and fourth bands and even promises the potential to identify Bruch's membrane band in the normal eye (green arrow in Figure 1(a2)).

AO-OCT of the outer retina

With improved spatial resolution, AO-OCT revealed a much thinner thickness of the second band compared to that in the clinical OCT (Figure 4). As shown in Figure 4, the second band thickness in the clinical OCT is consistent with the ISe thickness (16–20 μm), but AO-OCT measurement demonstrated that the second band thickness is much thinner,[2,25] only about 4.7 μm.[2] In

consideration of the broadening effect of axial point spread function (PSF), the actual axial extent of the second band's constituent interfaces was estimated at 3.5 μm, suggesting the second band originated from IS/OS junction.[2] The histologic examination, showing the distal IS membrane and the proximal OS membrane were separated by less than 3.5 μm, further supports this notion.[2] Moreover, AO-OCT measurement of individual photoreceptors revealed that the second band peak is closer to the third band than the first band. Based on these observations, it was proposed that the second band in AO-OCT reflects the IS/OS junction instead of the ISe.[2] It was reported that the third band thickness was around 4.3–6.4 μm in AO-OCT, but the third band thickness in clinical OCT was around 14–19 μm.[26] Consequently, the AO-OCT studies suggested that the band thickness in clinical OCT may be overestimated.
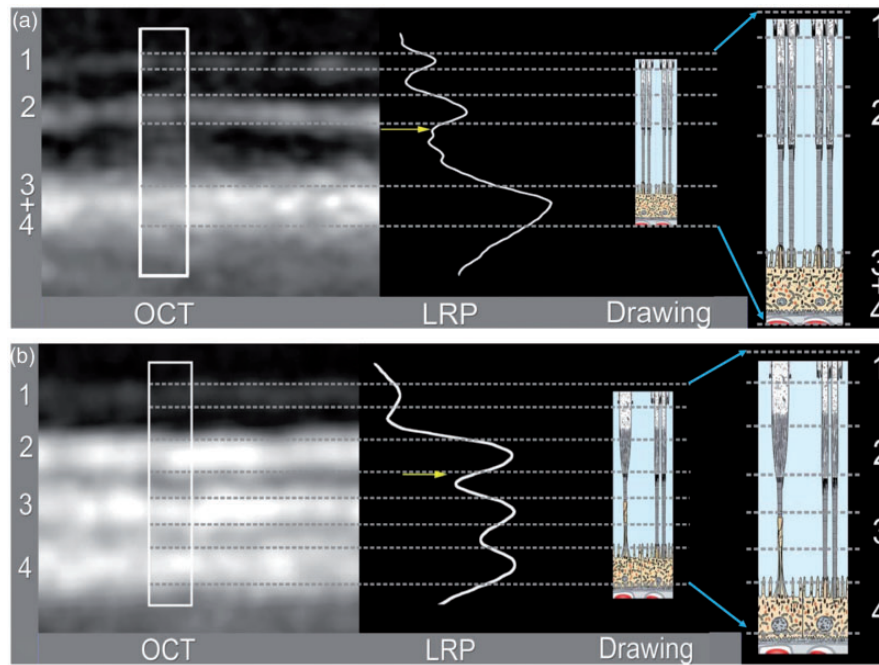
Figure 3. Comparative alignment of clinical OCT bands with the anatomically correct model at central foveal (a) and perifoveal (b) regions. (A color version of this figure is available in the online journal.)
OCT: optical coherence tomography; LRP: longitudinal reflectance profile.
Source: Modified with permission from Spaide and Curcio.[1]

Table 1. Summary of histological parameters of the outer retina.[1,24]

| Region	ISm length	ISe length	OS length	Supracone space
Central fovea	14 µm	20 µm	35 µm	1 µm
Parafovea	–	–	22 µm	–
Perifovea	13 µm	16 µm	6.5–13 µm	16 µm

ISe: inner segment ellipsoid; ISm: inner segment myoid; OS: outer segment.

Animal OCT of the outer retina

OCT studies using animal models have also been implemented to explore the anatomic sources of the outer retina.[21,22] A custom-built OCT with subcellular resolution (lateral: ~2 µm, axial: ~4 µm) has been used to characterize the outer retinal bands in excised living frog retinas.[21] Leopard frog (*Rana pipiens*) was selected due to its large photoreceptors (cone: ~3 µm, rod: ~6 µm),[27] enabling accurate OCT recording at sub-cellular resolution (Figure 5). Without complications of ocular aberrations and signal contamination from other ocular tissues, the animal OCT revealed individual photoreceptors and retinal layers with sufficient lateral and axial resolution.[21] Figure 5 illustrates comparative OCT (Figure 5(a)) and histological (Figure 5(b)) images of the outer retina of a frog eye. As shown in Figure 5(d), it was confirmed that the second band reasonably matches the ISe region.

Functional OCT was also employed for *in vivo* imaging of stimulus-evoked intrinsic optical signal (IOS) changes in the mouse retina.[22] Figure 6(a) shows representative OCT and IOS images, and visible light stimulation was delivered at the time 0. The spatiotemporal M-sequence in Figure 6(a1) indicates that the relative OCT band locations did not change in the pre-stimulus and post-stimulus periods. In contrast, IOS imaging, with background signal subtraction to enhance the visibility of transient light changes due to retinal stimulation, revealed robust intensity changes, particularly at the outer retina. As shown in Figure 6(a2), rapid IOS change was observed at the OS almost right after the stimulus, and the IOS change at the IS was relatively slow. Further analysis of OCT and IOS reflectance profiles in Figure 6(b) confirmed the different time courses between the OS-IOS and IS-IOS change. The rapid response of the OS-IOS is correlated with transient OS deformation, caused by phototransduction activation.[28–31] In contrast, the IS-IOS might reflect the metabolic activity of mitochondria, following the phototransduction in the OS. ISe has abundant mitochondria, a prominent light scatterer in the photoreceptor.[32] Under metabolic stress, the mitochondria are known to undergo morphological changes, i.e. fission and fusion, which can alter the refractive index[33–36] and subsequently cause IS-IOS changes. Therefore, the results shown in Figure 6 provide evidence that the ISe with highly packed mitochondria could be the primary source of the second band.
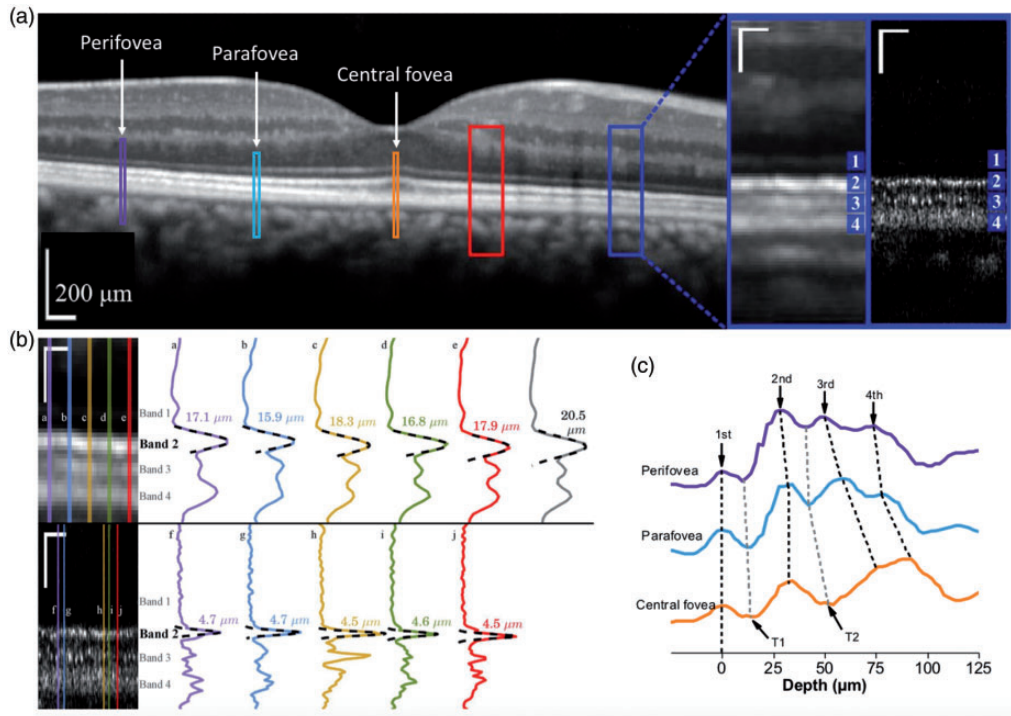
Figure 4. (a) Comparative clinical OCT and AO-OCT. Horizontal wide-field Spectralis B-scan centered on the fovea (left). Image is displayed on a logarithmic scale. Red and blue boxes indicate locations, 2.0° nasal and 5.0° nasal, used for AO-OCT imaging. Magnified view (near right) of the blue box containing outer retinal layers at 5.0° nasal, shown in linear scale. Corresponding AO-OCT image (far right) from the same location, shown in linear scale. (b) Band thickness measurement with Spectralis OCT and AO-OCT. A 210-μm wide section of a Spectralis B-scan (top left) acquired from a subject at 5.0° and converted to a linear intensity scale. The overlaid lines indicate the locations of the five A-scans plotted at (top right), labeled (a) to (e). The sixth (gray) plot represents the average of 10 A-scans. Dashed line overlaid on each plot is a least-squares Gaussian fit, from which the full-width at half-maximum (FWHM) of the peak can be readily calculated. A comparable AO-OCT B-scan (bottom left) from the same subject and eccentricity is also shown in linear scale. Locations for the plotted A-scans (bottom right), labeled f to j, were selected by identifying bright cones in the image. FWHM values were considerably smaller. Note that in both OCT and AO-OCT, averaging over multiple cells leads to an overestimate of layer thickness due to axial displacements of the reflections. Scale bars: 50 μm. (c) Reflectance profiles of the central fovea (yellow), parafovea (blue), and perifovea (purple) regions, corresponding to the yellow, blue, purple windows in the temporal region of image (a). In (c), the first band locations of three profiles are aligned together to show the relative position shifts of the second, third, and fourth bands. T1 and T2 indicate trough positions along the reflectance profiles. (A color version of this figure is available in the online journal.)
Source: (a) and (b) reprinted with permission from Jonnal et al.[2]

Comparative analysis of the outer retinal OCT bands

As shown in Figure 3, the anatomically correct model supports the ISe and IZ as the correlates of the second and third bands, respectively, in clinical OCT.[1] Comparative animal OCT studies also provide evidence for the contribution of the ISe to the second band (Figures 5 and 6).[21,22] In contrast, AO-OCT demonstrates that the IS/OS junction and OS tip are the correlates of the second and third bands, respectively (Figure 4). Two major differences were observed between AO-OCT and clinical OCT. First, the relative location of the band is different. In clinical OCT, the second band is unambiguously closer to the first band, i.e. the ELM, at the central fovea (Figures 1 and 3) suggesting ISe as the correlate of the second band. However, in AO-OCT, the second band is relatively closer to the third band. Second, the band thickness is different. In clinical OCT, the second and third bands have definite thicknesses. In contrast, the second and third band thickness in AO-OCT is typically around 4–5 μm, close to the axial PSF.

For a better understanding of these discrepancies between the clinical OCT and AO-OCT observations, we conducted a quantitative analysis of band positions. Table

2 provides a summary of the relative band positions of the outer retina at the central fovea, parafovea, and perifovea, from 12 OCT images acquired with the clinical OCT device (Optovue, Fremont, CA, USA) at the eye hospital of the University of Illinois at Chicago. The retrospective OCT study was approved by the Institutional Review Board (IRB) of the University of Illinois at Chicago (UIC) and complied with the ethical standards stated in the Declaration of Helsinki. Figure 7 illustrates representative reflectance profiles of OCT images from six subjects. The same parameters are also examined for the OCT images in Figures 1(a) and 4 (a) to verify the reliability of the analysis (Tables 3 and 4). The axial distance quantification in Table 4 is based on the scale bar provided in Figure 4(a), which allows the relative distance assessment among individual bands.

We found that the relative distances L_{1-2} and L_{2-3}, from the second band peak to the first and third band peaks, are 31.6 μm and 42.1 μm, respectively, at the central fovea (Table 2). Based on the 14 μm ISm and 20 μm ISe (Table 1), the second band peak is within the ISe, ~2.4 μm away from the IS/OS junction. In other words, relative distances from the second band peak to the ISm/ISe junction and IS/OS junction are ~17.6 μm (ISm: 14 μm; L_{1-2}: 31.6 μm) and ~2.4 μm (ISm: 14 μm, ISe: 20 μm, L_{1-2}: 31.6 μm),
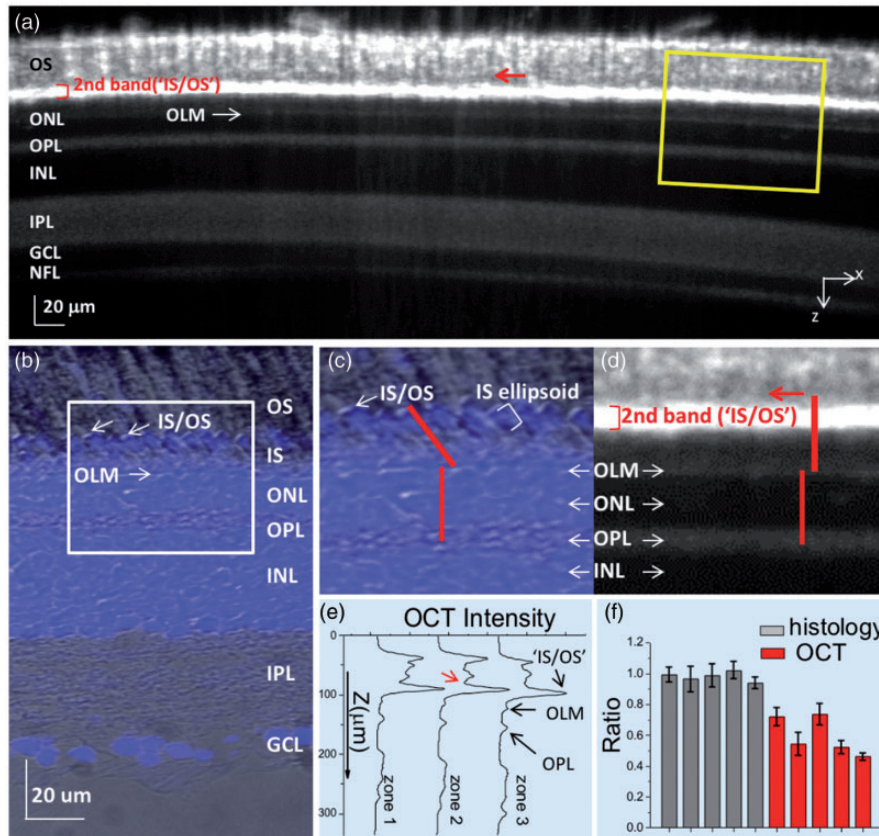
Figure 5. Comparative histology and OCT of the outer retina of a frog retina. (a) OCT B-scan. Red arrow points to a local hypo-reflective band. (b) Histological image. (c) Enlarged histological image marked by the white window in (b). (d) Enlarged OCT image marked by the yellow window in (a). (e) Representative OCT reflectance profiles over retinal depth. (f) Distance ratio in histological image ($H_{IS/OS}$–H_{OLM})/(H_{OLM}–H_{OPL}) and the OCT image ($OCT_{IS/OS}$–OCT_{OLM})/(OCT_{OLM}–OCT_{OPL}). Five samples were used for histological and OCT measurements, and for each sample, six positions were measured. Error bars indicate standard deviations. (A color version of this figure is available in the online journal.)

IS: inner segment; OCT: optical coherence tomography; OLM: outer limiting membrane; OS: outer segment; RPE: retinal pigment epithelium.
Source: Reprinted with permission from Lu et al.[21]

respectively. This observation indicates that the second band peak is within the ISe but closer to the IS/OS side. In addition, the relative distance D_{T1}, from the hypo-reflective T1 trough to the first band peak, is 14.3 µm. The 14.3 µm D_{T1} well matches the 14 µm ISm, indicating the OCT signal gradually increases from the T1 trough to the second band peak. These observations suggest that both the ISe and IS/OS junction can contribute to the second band in clinical OCT. The same trend is consistently observed in individual measurements in Tables 3 and 4.

In addition, the relative distances to the third band were analyzed. As shown in Table 2, the relative distance L_{1-3}, from the first to third bands, is 73.8 µm at the central fovea. By referring to the 14 µm ISm, 20 µm ISe, and 35 µm OS lengths summarized in Table 1, the total photoreceptor length is estimated to be ~69 µm at the central fovea.[1] Thus, the photoreceptor tip is expected within the third band, and the third band "peak" can be considered as a marker of the OS tip position. However, the third band in clinical OCT has a definite thickness. As shown in Table 2, the average distance D_{T2}, from the first band peak to the T2 band trough, is 47.8 µm. Because the IS length is 34 µm in Table 1 (14 µm ISm and 20 µm ISe), the 47.8 µm D_{T2} indicates that the T2 trough is within the OS, ~13.8 µm away from the

IS/OS junction. From the T2 trough, the OCT signal gradually increases to the third band peak. The transition range from the T2 trough to the third band peak is 26 µm (73.8 µm L_{1-3} and 47.8 µm D_{T2}), supporting that the OS tip is not the only contributor of the third band. In other words, both the OS tip and RPE apical processes interdigitated with the OS might contribute to the third band.[1,13] The same trend is confirmed in individual measurements in Tables 3 and 4.

We also found that the relative distances between hyper-reflective (first, second, third, and fourth) band peaks and hypo-reflective (T1, T2, T3) band troughs gradually change with increasing eccentricity (Figures 1(a2) and 4(c)). This can be explained by structural changes of the retinal photo-receptors and RPE apical processes. With increasing eccentricity, the cone IS becomes wider but slightly shorter, which is consistent with the reduced distance between the first and second band peaks at the parafovea and peri-fovea, compared to that at the central fovea. In Table 1, the IS length is slightly reduced from 34 µm (14 µm ISm and 20 µm ISe) at the central fovea to 29 µm (13 µm ISm and 16 µm ISe) at the perifovea. In contrast, the OS length is significantly reduced from 35 µm at the central fovea to 22 µm at the parafovea, and 6.5–13 µm at the perifovea. By considering the 29 µm IS and 6.5–13 µm OS at the perifovea,
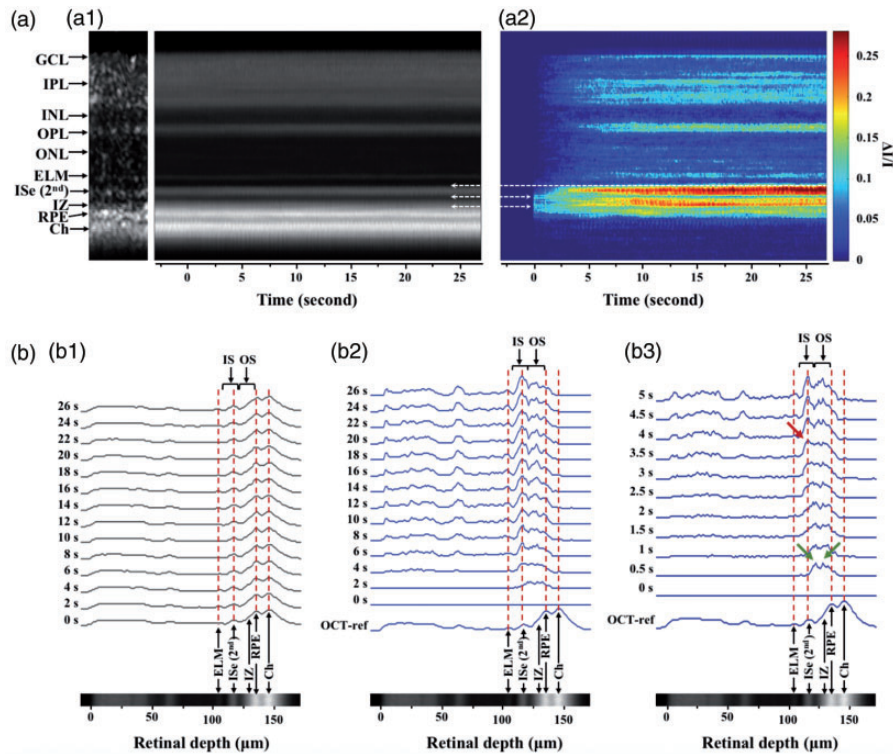
Figure 6. (a) OCT intensity (a1) and IOS activity (a2) M-scan maps. Three white arrows, from top to bottom along the direction of the inner to outer retina, show the top boundary of ISe (second), the connection between the ISe (second) and OS, and the connection between OS and RPE, respectively. (b) OCT intensity (b1) and IOS activity (b2) waveform of the M-scan at different time points. (b3) The early phase of B2. Green arrows show that the IOS change at the boundaries of the OS was stronger than the IOS change in the middle of the OS. The red arrow shows a peak response at the ISe (second) band at ~3.5 s. (A color version of this figure is available in the online journal.)

GCL: ganglion cell layer; IPL: inner plexiform layer; INL: inner nuclear layer; OPL: outer plexiform layer; ONL: outer nuclear layer; ELM: external limiting membrane; ISe (2nd): inner segment ellipsoid (the 2nd hyper-reflective band); IZ: interdigitation zone; RPE: retinal pigment epithelium; Ch: Choroid; IS: photoreceptor inner segment; OS: photoreceptor outer segment.

Source: Modified with permission from Ma et al.[22]

Table 2. Average band positions of 12 retinas.

| Region	L_{1-2} (μm)	L_{2-3} (μm)	L_{3-4} (μm)	L_{1-3} (μm)	D_{T1} (μm)	D_{T2} (μm)
Central fovea	31.6 ± 2.5	42.1 ± 2.7	15.3 ± 3.5	73.8 ± 3.5	14.3 ± 2.1	47.8 ± 2.4
Parafovea	31.1 ± 1.4	28.3 ± 4.8	18.4 ± 5.0	59.4 ± 5.5	11.8 ± 2.4	41.8 ± 2.7
Perifovea	28.6 ± 2.0	24.0 ± 3.1	19.9 ± 3.6	52.6 ± 3.7	11.4 ± 2.8	37.5 ± 2.0

L_{1-2}, L_{2-3}, L_{3-4}, and L_{1-3} are relative distance from the first to second, second to third, third to fourth, and first to third bands, respectively. D_{T1} and D_{T2} are the relative distances from the first band to the hyporeflective bands T1 and T2, respectively.

it might not be surprising for the second band to become closer to the third band, relative to the first band. In Table 2, the relative distance L_{3-4} between the third and fourth bands changes from 15.3 μm at the central fovea to 19.9 μm at the perifovea. The same trend is consistently observed in individual measurements in Tables 3 and 4. The increased L_{3-4} might reflect the eccentricity dependent changes of the supracone space and RPE apical process.[1] Moreover, recent studies of animal models also suggested that the hypo-reflective region between the third and fourth bands could be affected by the light condition.[37]

Discussion

In summary, four hyper-reflective bands are typically observed in clinical OCT of the outer retina. The first and

fourth bands are commonly attributed to the ELM and RPE/Bruch's complex, respectively. Continuous resolution improvement promises further separation of the fourth band into the RPE and Bruch's membrane (Figure 1). However, anatomic correlates of the second and third bands have been controversial, particularly the inconsistency observed in between clinical OCT and AO-OCT. The anatomically correct model supports that the second and third bands are attributed to the ISe and IZ, respectively. ISe is known to have abundant mitochondria which can work as light scatterer to contribute to the OCT signal. OCT studies using animal models have also provided evidence for the contribution of the ellipsoid on the second band.[21,22] In contrast, AO-OCT revealed a much thinner second band (4.7 μm) compared to that (16–20 μm) in clinical OCT. Moreover, the second band peak is closer to the third
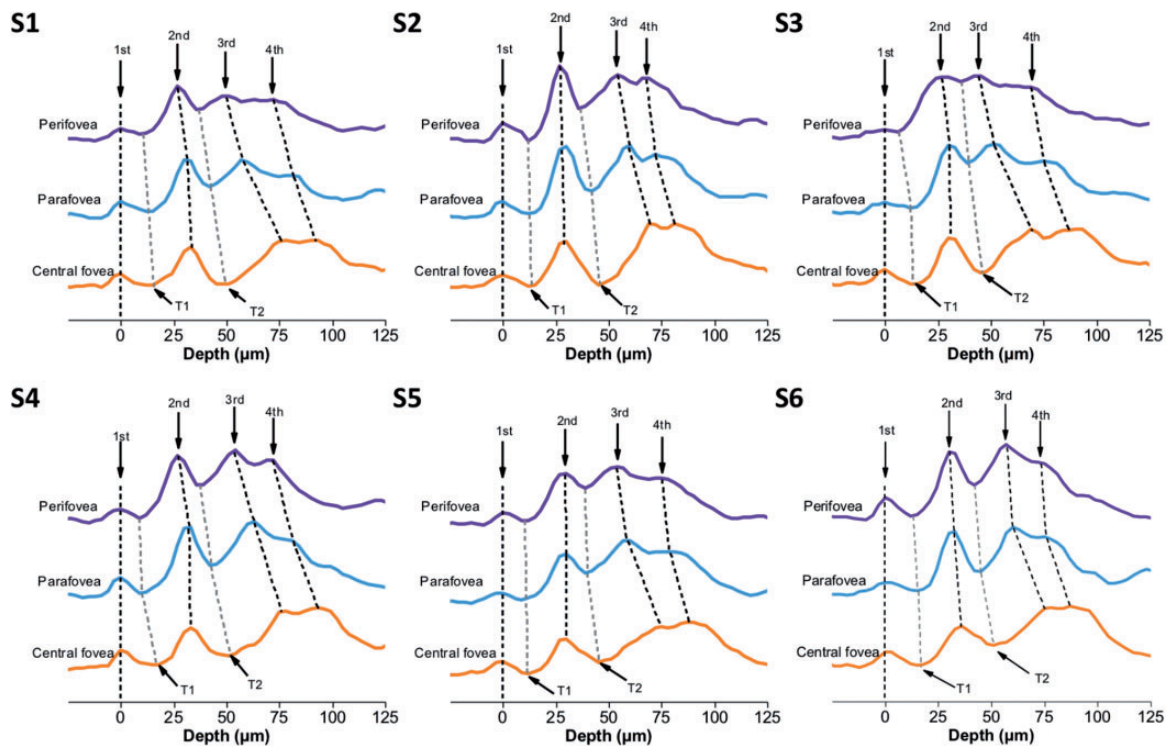
Figure 7. Representative reflectance profiles at central foveal, parafoveal, and perifoveal regions. All OCT images from six subjects (S1–S6) were acquired with a clinical OCT. (A color version of this figure is available in the online journal.)

Table 3. Relative band positions of the outer retina in OCT image of Figure 1(a).

Region	L_{1-2} (μm)	L_{2-3} (μm)	L_{3-4} (μm)	L_{1-3} (μm)	D_{T1} (μm)	D_{T2} (μm)
Central fovea	29	41	13	70	14	44
Parafovea	26	27	13	53	10	35
Perifovea	24	22	18	46	8	33

L_{1-2}, L_{2-3}, L_{3-4}, and L_{1-3} are relative distance from the first to second, second to third, third to fourth, and first to third bands, respectively. D_{T1} and D_{T2} are the relative distances from the first band to the hyporeflective bands T1 and T2, respectively.

Table 4. Relative band positions of the outer retina in OCT image of Figure 4(a).

| Region	L_{1-2} (μm)	L_{2-3} (μm)	L_{3-4} (μm)	L_{1-3} (μm)	D_{T1} (μm)	D_{T2} (μm)
Central fovea	33	43	14	76	15	53
Parafovea	31	28	20	59	13	42
Perifovea	28	22	24	50	10	41

L_{1-2}, L_{2-3}, L_{3-4}, and L_{1-3} are relative distance from the first to second, second to third, third to fourth, and first to third bands, respectively. D_{T1} and D_{T2} are the relative distances from the first band to the hyporeflective bands T1 and T2, respectively.

band, supporting that the second band is attributed to the IS/OS junction (Figure 4). A similar trend was also observed in the third band. The third band thickness was around 4.3–6.4 μm in AO-OCT, while the third band thickness in clinical OCT was around 14 to 19 μm.[26]

There are a few possible factors that could account for such different interpretations. First, the retinal region can significantly affect the relative band location. For the AO-OCT in Figure 4, the measurements were made at 2.0° and 5.0° retinal eccentricities.[2] Based on ~0.28 mm per visual angle, the 2.0° eccentricity corresponds to a ~0.56 mm distance from the center of the fovea, which is a retinal region beyond the foveola (~0.35 mm diameter region at the central fovea) and foveal avascular zone (~0.5 mm diameter

region at the central fovea) in the normal eyes (Figure 8). The 5.0° eccentricity corresponds to a perifoveal region. In contrast, the central fovea measurement in clinical OCT corresponds to the exact center of the fovea (Figure 3), i.e. the umbo region where only cones are densely packed (Figure 8(c)).[3] The cone IS and OS lengths are 34 and 35 μm, respectively, at the central fovea. In contrast, the cone IS and OS lengths are 29 and 6.5–13 μm, respectively, at the perifovea. In other words, the ratio of IS/OS length at the central fovea can be very different from other regions. Thus, the disagreement about the second band location, relative to first and third bands, was most likely due to the different retinal regions for the OCT images in Figures 3 and 4.
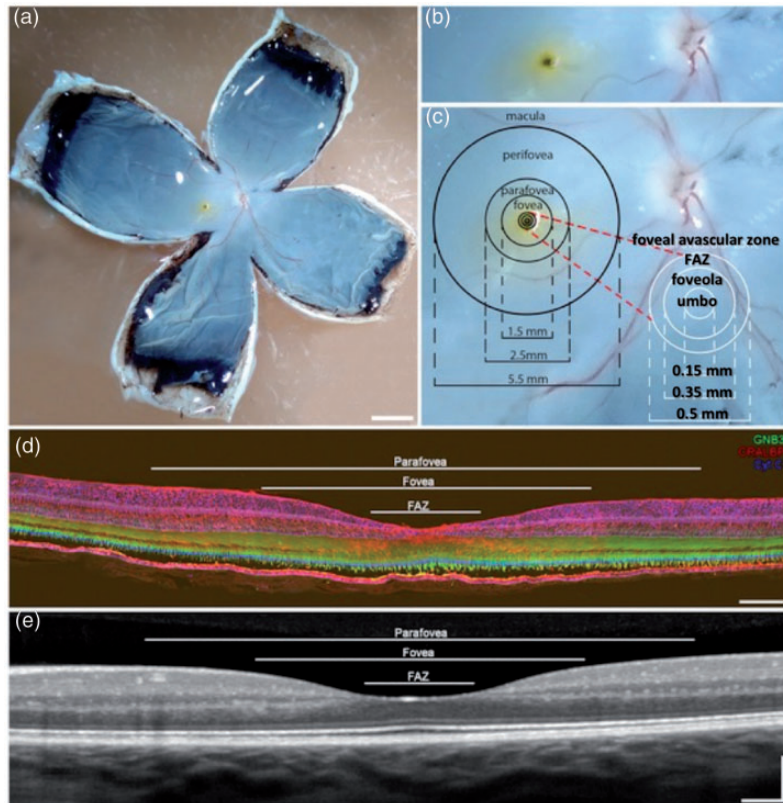
Figure 8. Human macular anatomy. Dissected human eye in which the macula, its different regions, and the optic nerve head can be seen. This eye was treated with RNA-later© for its preservation, which changes the typical translucent appearance of the retina to a white coloration, allowing for a clearer view of the yellow pigment (a). Magnification image of macular zone (b and c) indicating each of the macular region dimensions (c). Dimensions of macular regions at a retinal section (stained with GNB3, CRALBP, and cytochrome-C antibodies) (d) and its correlation with an OCT image at the same area (e). Scale bars: (a) 5 mm; (d) 200 μm; (e) 200 μm. (A color version of this figure is available in the online journal.)
Source: Reprinted with permission from Cuenca et al.[3]

Second, the confounding effect should be considered in clinical OCT interpretations. Our quantitative analysis indicates that the second band peak in clinical OCT is located between the ISm/ISe junction and IS/OS junction, but closer to the IS/OS junction side (Table 2). This demonstrates that both ISe and IS/OS junction can simultaneously contribute to the second band in clinical OCT. Moreover, it should be noted that the connecting cilium (CC) is another potential contributor to the second band.[38] Although the CC was speculated to be too small to be visible in OCT,[1] the OCT as in the light microscopy can pick up the signal from any scatters with dimensions smaller than the system resolution. Subcellular bright autofluorescence spots, which might relate to CC in cone photoreceptors, have been observed in freshly isolated retinas,[38] and in vivo super-resolution imaging revealed similar subcellular bright structures in frog photoreceptors (Figure 9).[39] Further verification of the effect to the CC on OCT is required to validate the CC as one of the major contributors to the second band. Similarly, the confounding effect on the third band should be noted. Relative distance L_{1-3}, between the first and third bands, well matches the IS+OS length, supporting the third band peak can reflect the position of OS tips (Table 2). However, the possible contribution from the IZ to the third band could not be excluded solely based on the peak position, given the transition range 26 μm, from

the T2 trough to the third band peak, as well as the definite thickness of the third band. In fact, the third band is the most controversial band among researchers, and multiple interpretations for this zone have been proposed.[1,3] Thus, it would be reasonable to consider that multiple sources, such as RPE apical processes, OS tip, and even OS itself, can contribute to the third band,[2,3] instead of identifying a single correlate exclusively for the third band.

Lastly, the different imaging sensitivities of the AO-OCT and clinical OCT can affect the observed second and third band thickness. Although there is no doubt that AO-OCT can provide improved spatial resolution compared to conventional OCT, the AO-OCT might selectively enhance the visibility of a structure within the focusing center. In contrast, the light efficiency for detecting the structures outside of the focal plane can be quickly degraded. This effect can be directly observed in Figure 4(b). As shown in Figure 4, the clinical OCT clearly reveals all outer retinal bands (Figure 4(b), (a) to (e)). However, only the second band exhibits a good signal-to-noise ratio in AO-OCT (Figure 4 (b), (f) to (j)). Particularly, the first band is absent in AO-OCT, and it is also difficult to identify the peak locations and widths of the third and fourth bands (Figure 4(b), (f) to (j)). One possible reason to cause this difference might be the effect of the effective numerical aperture (NA). For the AO-OCT, the 2.5 μm lateral resolution requires a 6.75 mm
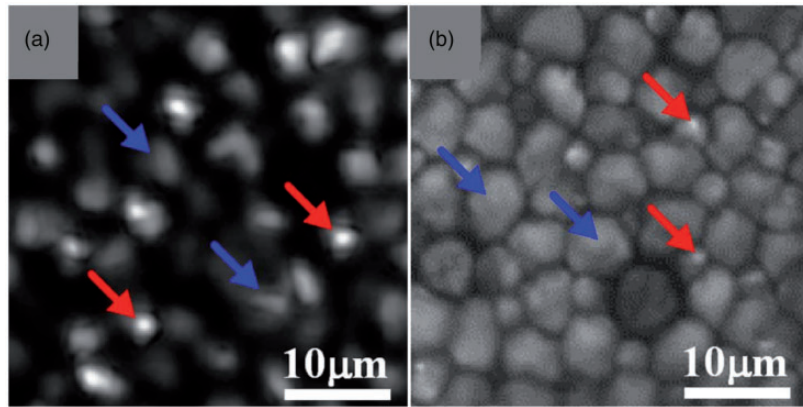
Figure 9. (a) In vivo super-resolution imaging of scattering light in frog photoreceptors. (b) Comparative two-photon excited autofluorescence imaging of frog retina. Blue arrowheads indicate rods, while red arrowheads indicate cones. Super bright spots are observed as a subcellular structure in retinal photoreceptors. (A color version of this figure is available in the online journal.)
Source: Reprinted with permission from Zhi et al.[39]

pupil diameter of the eye, corresponding to an effective NA = 0.2. If we assume a 10 µm lateral resolution in clinical OCT, it corresponds to an effective NA = 0.05. It is well established that a higher NA corresponds to a shaper focusing property but a shallow depth-of-field. Moreover, the AO is based on dynamic sensing and correction of wavefront distortions. Reliable sensing of the wavefront information requires robust mapping of the reflectance profile of the target. When the AO-OCT is focusing to a relatively flat region, such as the IS/OS junction, or a strong scatterer with sufficient brightness compared to background light intensity, the wavefront sensing and correction can be effective based on the phase information carried by the ballistic photons. However, if the AO-OCT is focusing within a region consisting of moderate scatters such as mitochondria, this multiply scattered light can produce diffusive photons, which might randomize the phase information among different photons to affect the wavefront sensing and correction in the AO system. Therefore, it is possible for the AO-OCT to selectively enhance the sensitivity for imaging ballistic photons from the IS/OS junction, while partially rejecting the diffusive photons within the ISe region, with the higher sectioning capability of the AO-OCT compared to clinical OCT.

Conclusions

Photoreceptor ISe and IS/OS junction can contribute to the second band; OS, OS tips, and RPE apical processes can contribute to the third band in clinical OCT. These signal sources might contribute to the signal detection in clinical OCT and AO-OCT at different weighting factors, due to the different system resolution, aberration, effective pupil size, illumination, imaging orientation, and perhaps other factors. AO-OCT might selectively enhance the detection sensitivity of the ballistic photons from the IS/OS junction and OS tips while minimizing the detection sensitivity of the diffusive photons from the ISe, RPE apical processes, and OS, which can differentiate the second and third band characteristics from clinical OCT. Therefore, the possibility of multiple contributors for the clinical OCT should not be

overlooked, and the contributing factors of individual correlates can be variable in different instruments, testing protocols, and eye conditions. In addition, relative band locations should be discussed under the context of specific retinal regions, since the anatomy of the photoreceptor cells is significantly varied with increasing eccentricity.

AUTHORS' CONTRIBUTIONS

XY drafted the manuscript. DL and TS contributed to figure preparation. TK contributed to the manuscript and figure preparation.

DECLARATION OF CONFLICTING INTERESTS

The author(s) declared no potential conflicts of interest with respect to the research, authorship, and/or publication of this article.

ORCID iDs

Xincheng Yao https://orcid.org/0000-0002-0356-3242
Taeyoon Son https://orcid.org/0000-0001-7273-5880
Tae-Hoon Kim https://orcid.org/0000-0002-4391-4860
David Le https://orcid.org/0000-0003-3772-1875

REFERENCES

1. Spaide RF, Curcio CA. Anatomical correlates to the bands seen in the outer retina by optical coherence tomography: literature review and model. *Retina* 2011;**31**:1609–19
2. Jonnal RS, Kocaoglu OP, Zawadzki RJ, Lee SH, Werner JS, Miller DT. The cellular origins of the outer retinal bands in optical coherence tomography images. *Invest Ophthalmol Vis Sci* 2014;**55**:7904–18
3. Cuenca N, Ortuno-Lizaran I, Sanchez-Saez X, Kutsyr O, Albertos-Arranz H, Fernandez-Sanchez L, Martinez-Gil N, Noailles A, Lopez-Garrido JA, Lopez-Galvez M, Lax P, Maneu V, Pinilla I. Interpretation of

OCT and OCTA images from a histological approach: clinical and experimental implications. *Prog Retin Eye Res* 2020;**77**:100828

4. Drexler W, Sattmann H, Hermann B, Ko TH, Stur M, Unterhuber A, Scholda C, Findl O, Wirtitsch M, Fujimoto JG, Fercher AF. Enhanced visualization of macular pathology with the use of ultrahigh-resolution optical coherence tomography. *Arch Ophthalmol* 2003;**121**:695–706

5. Kolb H. *Simple anatomy of the retina by Helga Kolb*, http://webvision.med.utah.edu/book/part-i-foundations/simple-anatomy-of-the-retina/ (accessed 1 May 2021)

6. Omri S, Omri B, Savoldelli M, Jonet L, Thillaye-Goldenberg B, Thuret G, Gain P, Jeanny JC, Crisanti P, Behar-Cohen F. The outer limiting membrane (OLM) revisited: clinical implications. *Clin Ophthalmol* 2010;**4**:183–95

7. Woronkowicz M, Lightman S, Tomkins-Netzer O. The prognostic value of total macular external limiting membrane and ellipsoid zone damage for clinical outcome in treatment-resistant neovascular age-related macular degeneration. *Graefes Arch Clin Exp Ophthalmol* 2020;**258**:2373–8

8. Chhablani JK, Kim JS, Cheng L, Kozak I, Freeman W. External limiting membrane as a predictor of visual improvement in diabetic macular edema after pars plana vitrectomy. *Graefes Arch Clin Exp Ophthalmol* 2012;**250**:1415–20

9. De S, Saxena S, Kaur A, Mahdi AA, Misra A, Singh M, Meyer CH, Akduman L. Sequential restoration of external limiting membrane and ellipsoid zone after intravitreal anti-VEGF therapy in diabetic macular oedema. *Eye* 2021;**35**:1490–5

10. Lee W, Noupuu K, Oll M, Duncker T, Burke T, Zernant J, Bearelly S, Tsang SH, Sparrow JR, Allikmets R. The external limiting membrane in early-onset Stargardt disease. *Invest Ophthalmol Vis Sci* 2014;**55**:6139–49

11. Ding X, Zhan Z, Sun L, Yang Y, Li S, Zhang A, Luo X, Lu L. Retinal pigmental epithelium elevation and external limiting membrane interruption in myopic choroidal neovascularization: correlation with activity. *Graefes Arch Clin Exp Ophthalmol* 2018;**256**:1831–7

12. Landa G, Gentile RC, Garcia PM, Muldoon TO, Rosen RB. External limiting membrane and visual outcome in macular hole repair: spectral domain OCT analysis. *Eye (Lond)* 2012;**26**:61–9

13. Staurenghi G, Sadda S, Chakravarthy U, Spaide RF, International Nomenclature for Optical Coherence Tomography (IN-OCT) Panel. Proposed lexicon for anatomic landmarks in normal posterior segment spectral-domain optical coherence tomography: the in*OCT consensus. *Ophthalmology* 2014;**121**:1572–8

14. Chong SP, Zhang T, Kho A, Bernucci MT, Dubra A, Srinivasan VJ. Ultrahigh resolution retinal imaging by visible light OCT with longitudinal achromatization. *Biomed Opt Express* 2018;**9**:1477–91

15. Adhi M, Read SP, Liu JJ, Fujimoto JG, Duker JS. High-speed ultrahigh-resolution OCT of Bruch's membrane in membranoproliferative glomerulonephritis type 2. *Ophthalmic Surg Lasers Imaging Retina* 2014;**45**:614–7

16. Inoue M, Arakawa A, Yamane S, Kadonosono K. Imaging of sub-retinal pigment epithelial linear structures in patients with age-related macular degeneration. *Eur J Ophthalmol* 2014;**24**:744–50

17. Bloom SM, Singal IP. The outer Bruch membrane layer: a previously undescribed spectral-domain optical coherence tomography finding. *Retina* 2011;**31**:316–23

18. Ohno-Matsui K, Jonas JB, Spaide RF. Macular Bruch membrane holes in choroidal neovascularization-related myopic macular atrophy by swept-source optical coherence tomography. *Am J Ophthalmol* 2016;**162**:133–9.e1

19. Park SP, Chang S, Allikmets R, Smith RT, Burke TR, Gregory-Roberts E, Tsang SH. Disruption in Bruch membrane in patients with Stargardt disease. *Ophthalmic Genet* 2012;**33**:49–52

20. Curcio CA. Johnson M. Structure, function, and pathology of Bruch's membrane. In: Retina. 5th ed. Amsterdam: Elsevier Inc, 2012, pp.465–81

21. Lu RW, Curcio CA, Zhang Y, Zhang QX, Pittler SJ, Deretic D, Yao XC. Investigation of the hyper-reflective inner/outer segment band in optical coherence tomography of living frog retina. *J Biomed Opt* 2012;**17**:060504

22. Ma G, Son T, Kim TH, Yao X. In vivo optoretinography of phototransduction activation and energy metabolism in retinal photoreceptors. *J Biophotonics* 2021;e202000462

23. DeRamus ML, Stacks DA, Zhang Y, Huisingh CE, McGwin G, Pittler SJ. GARP2 accelerates retinal degeneration in rod cGMP-gated cation channel beta-subunit knockout mice. *Sci Rep* 2017;**7**:42545

24. Stockman A. *Outer segment length of human photoreceptors*, http://www.cvrl.org/database/text/intros/introlength.htm (accessed 1 May 2021)

25. Meadway A, Girkin CA, Zhang Y. A dual-modal retinal imaging system with adaptive optics. *Opt Express* 2013;**21**:29792–807

26. Jonnal RS, Gorczynska I, Migacz JV, Azimipour M, Zawadzki RJ, Werner JS. The properties of outer retinal band three investigated with adaptive-optics optical coherence tomography. *Invest Ophthalmol Vis Sci* 2017;**58**:4559–68

27. Nilsson SE. An electron microscopic classification of the retinal receptors of the leopard frog (*Rana pipiens*). *J Ultrastruct Res* 1964;**10**:390–416

28. Lu Y, Wang B, Pepperberg DR, Yao X. Stimulus-evoked outer segment changes occur before the hyperpolarization of retinal photoreceptors. *Biomed Opt Express* 2017;**8**:38–47

29. Pandiyan VP, Maloney-Bertelli A, Kuchenbecker JA, Boyle KC, Ling T, Chen ZC, Park BH, Roorda A, Palanker D, Sabesan R. The optoretinogram reveals the primary steps of phototransduction in the living human eye. *Sci Adv* 2020;**6**:eabc1124

30. Lu Y, Benedetti J, Yao X. Light-induced length shrinkage of rod photoreceptor outer segments. *Transl Vis Sci Technol* 2018;**7**:29

31. Yao X, Kim TH. Fast intrinsic optical signal correlates with activation phase of phototransduction in retinal photoreceptors. *Exp Biol Med (Maywood)* 2020;**245**:1087–95

32. Cuenca N, Ortuño-Lizarán I, Pinilla I. Cellular characterization of OCT and outer retinal bands using specific immunohistochemistry markers and clinical implications. *Ophthalmology* 2018;**125**:407–22

33. Tychinsky V. The metabolic component of cellular refractivity and its importance for optical cytometry. *J Biophotonics* 2009;**2**:494–504

34. Tychinsky V, Kretushev A, Vyshenskaja T. Mitochondria optical parameters are dependent on their energy state: a new electrooptical effect? *Eur Biophys J* 2004;**33**:700–5

35. Westermann B. Mitochondrial fusion and fission in cell life and death. *Nat Rev Mol Cell Biol* 2010;**11**:872–84

36. Haseda K, Kanematsu K, Noguchi K, Saito H, Umeda N, Ohta Y. Significant correlation between refractive index and activity of mitochondria: single mitochondrion study. *Biomed Opt Express* 2015;**6**:859–69

37. Berkowitz BA, Podolsky RH, Qian H, Li Y, Jiang K, Nellissery J, Swaroop A, Roberts R. Mitochondrial respiration in outer retina contributes to light-evoked increase in hydration in vivo. *Invest Ophthalmol Vis Sci* 2018;**59**:5957–64

38. Lu RW, Li YC, Ye T, Strang C, Keyser K, Curcio CA, Yao XC. Two-photon excited autofluorescence imaging of freshly isolated frog retinas. *Biomed Opt Express* 2011;**2**:1494–503

39. Zhi Y, Lu R, Wang B, Zhang Q, Yao X. Rapid super-resolution line-scanning microscopy through virtually structured detection. *Opt Lett* 2015;**40**:1683–6